analytical chemistry

pubs.acs.org/ac Article

Plasmonic Enhanced Gold Nanoclusters-Based Photoelectrochemical Biosensor for Sensitive Alkaline Phosphatase Activity Analysis

Chun-Qin Zhao, Jing Zhou, Kai-Wen Wu, Shou-Nian Ding,* Jing-Juan Xu, and Hong-Yuan Chen

Cite This: *Anal. Chem.* 2020, 92, 6886−6892 Read Online

ACCESS | Metrics & More | Article Recommendations | Supporting Information

ABSTRACT: Low-toxicity gold nanoclusters-decorated Ag@SiO_2 (Au NCs-Ag@SiO_2) nanocomposites modified plasmonic photoelectrodes were first fabricated to improve the photoelectric properties of Au NCs and practical application in biological detection. Through adjusting distance between Au NCs and plasmonic silver nanoparticles (Ag NPs), the photocurrent intensity of Au NCs enhanced by 3.8 times attributed to strong competition between enhancement functions of hot electron transfer, local electric field, light scattering effects, and quenching functions of nonradiative energy transfer. Further comparison between experimental results and theoretical simulations were conducted to gain a deeper understanding toward the photoelectric enhancement mechanism. Moreover, Au NCs-Ag@SiO_2 nanocomposites was successfully applied to the construction of photoelectrochemical (PEC) biosensors for sensitively detecting alkaline phosphatase activity. This proposed PEC biosensor showed a wide linear range from 0.04 to 400 U·L^{-1}, and a low detection limit of 0.022 U·L^{-1}.

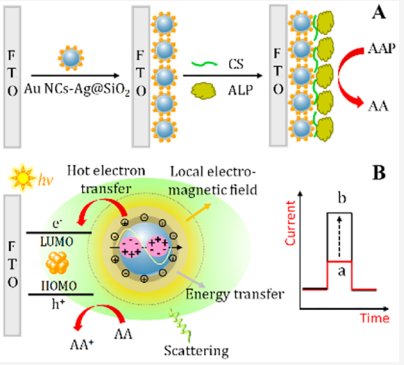

PEC bioanalysis has attracted substantial attention due to its higher sensitivity than traditional electrochemical methods, owing to the lower background effect, as well as simpler, cheaper, and easier to miniaturize apparatus than the optical method.[1−3] Notably, the properties of photoactive materials directly determine the PEC efficiency which are usually confirmed through photocurrent intensity, will further influence the detection sensitivity in PEC assay system. Semiconductor quantum dots (QDs) have become a class of versatile and extensively utilized photoactive materials due to their unique electronic and optical properties.[4,5] However, commonly used QDs often contain toxic elements which are harmful for biological samples and further restrict their applications in the PEC bioanalysis. In this regard, research on more photoactive nanomaterials with lower toxicity and higher photoelectric conversation efficiency are highly needed. Au NCs with low-toxicity and biocompatibility have been endowed with many fascinating semiconductive features which are similar to QDs owing to their molecular organometallic complex-like photophysical properties.[6−8] Meanwhile, it has been proved that Au NCs possess nice photostability and photocatalytic properties.[9] However, the produced photocurrent response of Au NCs alone is usually hard to meet the need of highly sensitive detection. Thus, it is of great importance to improve the photoelectric performance and further give full play to the advantages of Au NCs.

Metal (e.g., Au, Ag, Al, and Pt) nanostructures have been endowed with excellent electronic and optical characteristics owning to their distinctive localized surface plasmon resonance (LSPR) effect. Recently, direct plasmon-improved electrochemical detections based on high energy of LSPR excitation have been observed. Considering this process required certain voltage bias, further exploring toward the enhancement effects of plasmonic metals are still needed.[10−12] Especially, the combination of plasmonic metals with semiconductors have been regarded as a promising way to improve the photocatalytic activity and photocurrent response of semiconductor nanomaterials.[13,14] Correspondingly, most reported research was commonly based on plasmonic metals and semiconductors contacted directly. However, the nonradiative energy transfer from the photoexcited semiconductor to metal nanoparticles may quench the photoexcited semiconductor nanoparticles (NPs) at a close distance.[15,16] Recent studies have confirmed that the photoelectric activity of semiconductors were still enhanced even when insulated-spacers were presented between the metal and the semiconductor.[17−20] Generally, the significantly improved photoelectric properties were mainly ascribed to the fact that LSPR-mediated local electric field can increase the absorption efficiency of nearby semiconductor, and the light scattering effect can improve the light harvesting efficiency.[21,22] Therefore, the association of plasmonic metals

Received: December 1, 2019
Accepted: April 22, 2020
Published: April 22, 2020

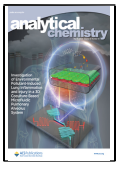

with Au NCs will be a judicious means to improve the photoelectric properties of Au NCs. Simultaneously, the best photoelectric activity will be expected to be achieved in an optimized distance, owing to the intensity of hot electron transfer, local electric field, light scattering effects, and nonradiative energy transfer changes along with the distance.[23,24] To date, only sporadic reports have studied plasmonic sensitization of Au NCs-semiconductor in ternary systems.[25,26] Despite the progress, systematic studies on photoelectric mechanism of plasmonic metal toward Au NCs to achieve optimal photoelectric properties and further application in bioanalysis are still needed.

Herein, low-toxicity Au NCs-Ag@SiO_2 nanocomposites with improving photoelectric performance were prepared. Meanwhile, to achieve maximum photocurrent enhancement, the distance between Au NCs and Ag NPs was optimized by adjusting the silica shell thickness. Additionally, the experimental results and theoretical simulations showed that the reinforcing functions of hot electron transfer, local electromagnetic field, light scattering effects, and the quenching functions of energy transfer plays diverse roles in different distances (Scheme. 1B). Furthermore, Au NCs-Ag@SiO_2 nanocomposites were utilized as the photoactive material to construct a novel PEC biosensing platform for alkaline phosphatase (ALP) activity assay (Scheme. 1A) based on the generation of electron donors (ascorbic acid, AA) in situ via the ALP catalytic chemistry.[27,28] More importantly, this research provided a foundation for designing green and convenient signal-on PEC sensing platforms.

Scheme 1. Schematic Illustration of (A) the Preparation Process of Au NCs-Ag@SiO_2 Nanohybrids, (B) Energy Diagram of LSPR Induced Photoelectric Enhancement System

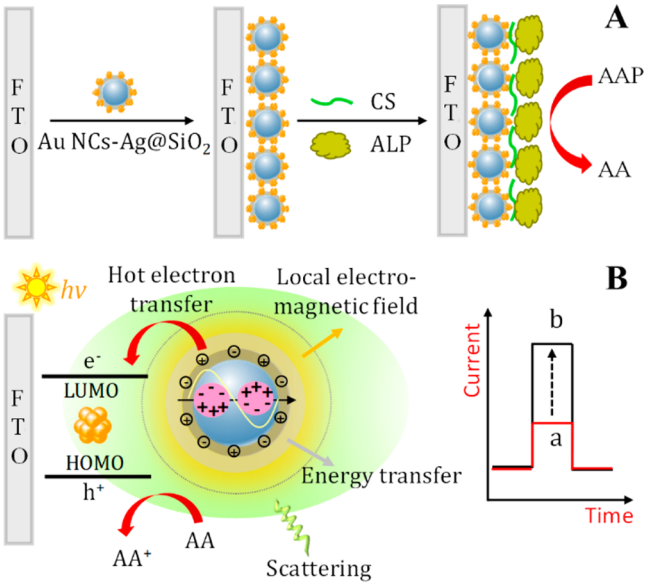

EXPERIMENTAL SECTION

Reagents and Apparatus. All chemicals and reagents were of analytical grade and were used without further purification. We purchased 3-aminopropyltrimethoxysilane (APTMS, 97%), AA from Sigma-Aldrich. ALP, Ascorbic acid phosphate (AAP) were obtained from Yuanye Biotech Co., Ltd. (Shanghai, China). Phosphate buffer solutions (PBS, 0.1 M, pH 7.4) were freshly prepared from 0.2 M of sodium dihydrogen phosphate ($NaH_2PO_4{\cdot}2H_2O$) and disodium hydrogen phosphate ($Na_2HPO_4{\cdot}12H_2O$). Electrochemical impedance spectroscopy (EIS) characterization was performed in ferrocyanide/ferricyanide solution (0.1 M KCl, 5 mM $Fe(CN)_6^{3-/4}$). For the performance studies of nanomaterials, PEC measurement was carried out in 0.1 M PBS containing 0.1 M AA. For the detections for alkaline phosphatase, the prepared sensing platform was first incubated in PBS containing 50 mM AAP at 37 °C for 40 min, and the photocurrent intensity was measured in the above buffer.

All PEC measurements were performed on a CHI 660E electrochemical workstation (Shanghai Chenhua Instrument Co., Ltd., China) with a PEC-A system (Wuhan Huachuang Hengsheng Technology Co., Ltd., China) employing LED as excitation source. Meanwhile, PEC measurements were carried out in a cell with a common three-electrode system consisting of a modified FTO electrode as a working electrode, platinum (Pt) wire as a counter electrode, and saturated calomel electrode (SCE) as a reference electrode under irradiation of 460 nm light with an applied potential of 0 V. All theoretical simulations were performed with finite-difference time-domain (FDTD) solutions (Lumerical Solutions, Inc., Canada) by applying plane-wave source of 460 nm, mesh sizes of 0.5 nm (x, y, z) for monomeric Ag@SiO_2 NPs and 1 nm (x, y, z) for dimers, X min boundary condition of anti-symmetric, Y min boundary condition of Symmetric, and others of PML. Other reagents and apparatus are depicted in the Supporting Information (SI).

Preparation of Au NCs-Ag@SiO_2 NPs. Ag NPs were synthesized via a previously reported citrate reduction method.[29] Core−shell Ag@SiO_2 NPs with different silica (SiO_2) thickness were conducted by the modified Stŏber method.[30] Glutathione protected Au NCs (GSH-Au NCs) were synthesized based on the literature report by Luo et al. with a slight modification.[31] More details are shown in the SI. Finally, after Ag@SiO_2 NPs were amino-functionalized (Ag@SiO_2−NH_2 NPs),[32] 300 μL colloidal solution were added to 200 μL aqueous solution of Au NCs (1 mg·mL^{-1}), and then were diluted to 1 mL with deionized water. The aqueous dispersion was shaken at room temperature for 3 h to obtain Au NCs-decorated Au@SiO_2 NPs (denoted as Au NCs-Ag@SiO_2).

Fabrication of photoelectrodes and PEC Measurements. Prior to use, fluorine-doped tin oxide (FTO) were ultrasonically cleaned by acetone, ethanol, and deionized water, respectively. Au NCs-Ag@SiO_2/GCE was obtained by dropping 10 μL of homogeneous solution onto the cleaned FTO electrode (0.5 cm in diameter) surface and drying at room temperature for further measurement and modification. For the fabrication of PEC sensing platform, 10 μL of chitosan (CS) solution (0.1 wt %) was spread onto the modified electrode and dried at room temperature. After being rinsed, the electrode was incubated in 10 μL of 2.5 wt % glutaraldehyde (GLD) solution for the following ALP linking. After removing of excessive GLD, 10 μL of ALP was dropped on the electrode surface and incubated for 4 h at 4 °C. After the modification processes, the prepared electrode was washed with buffer to remove physically adsorbed ALP. The modified electrode was marked as ALP/Au NCs-Ag@SiO_2/GCE, and stored at 4 °C before further use.

https://dx.doi.org/10.1021/acs.analchem.9b05432
Anal. Chem. 2020, 92, 6886−6892

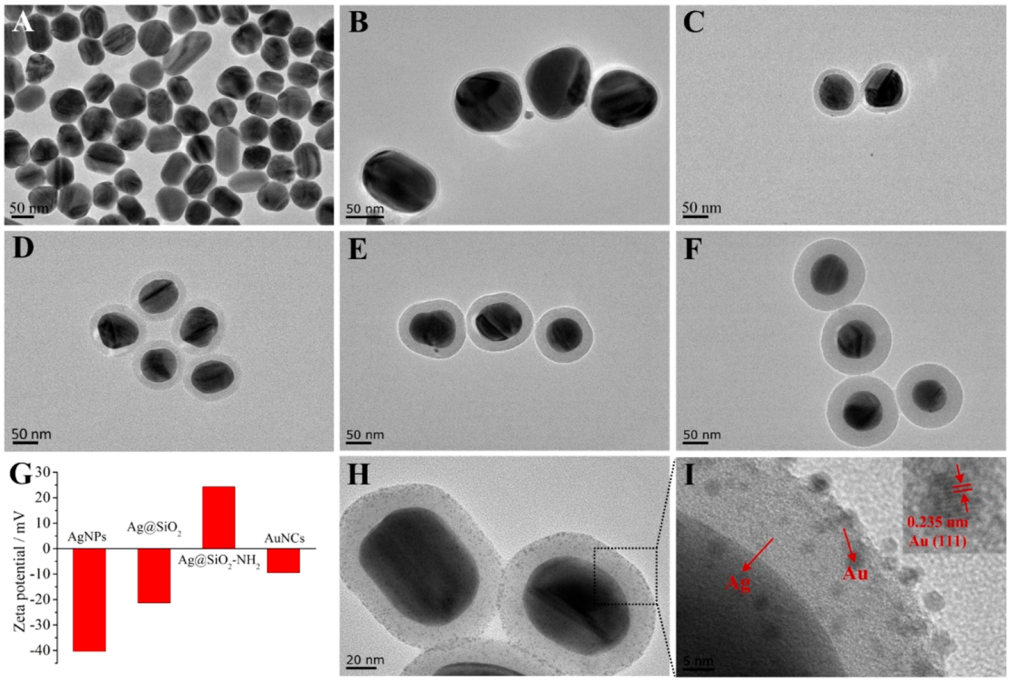

Figure 1. TEM images of $Ag@SiO_2$ NPs with different silica shell thicknesses (nm): (A) 0, (B) 5, (C) 10, (D) 15, (E) 20, (F) 30. (G) Zeta potentials of Ag NPs, $Ag@SiO_2$, $Ag@SiO_2$–NH_2, and Au NCs. (H) TEM and (I) HRTEM image of Au NCs-$Ag@SiO_2$ nanohybrids with the silica shell of 15 nm. The inset image: enlarged HRTEM of Au NCs.

RESULTS AND DISCUSSION

Characterizations of Nanomaterials. The formation of Ag NPs was characterized by the TEM images. As shown in Figure 1A, the TEM images of Ag NPs showed a quasi-spherical structure with an average diameter of 75 nm. When the surfaces of Ag NPs were coated with silica shells, a strong contrast between the black Ag cores and gray silica shells was presented, since the different electron density between them (Figure 1B–F). Noteworthy, the structure of $Ag@SiO_2$ NPs with different silica shell thicknesses (5, 10, 15, 20, and 30 nm) could tune the distance between the Ag NPs and the Au NCs. The TEM images of Au NCs and optical properties characterizations of nanomaterials are shown in SI Figure S1. The binding between Au NCs and $Ag@SiO_2$ was monitored through zeta potential measurements and TEM. From the data in Figure 1G, citrate protected Ag NPs showed a negative charge of −40.3 mV. The zeta potential of $Ag@SiO_2$ moved to −21.3 mV owning to the silanol groups on the surfaces. After animation, the zeta potential of $Ag@SiO_2$ changed to a positive charge of 24.3 mV due to the presence of an amino group. Conversely, the zeta potential of Au NCs showed a negative charge of −9.4 mV, since rich carboxyl groups were on the Au NCs surface. The potential difference between $Ag@SiO_2$–NH_2 (positive) and Au NCs (negative) revealed that the construction of $Ag@SiO_2$–Au NCs nanocomposite was feasible through the electrostatic interaction. As shown in Figure 1H–I and SI Figure S1C, the gray and smooth silica shells turned darker in color and turned rougher in appearance noticeably when compared with TEM images of $Ag@SiO_2$ alone. Additionally, the lattice fringe spacings of 0.235 nm in the inset image of Figure 1I corresponding to the (111) crystal plane of Au. These illustrated that the Au NCs were successfully anchored on the surface of $Ag@SiO_2$ NPs.

PEC Properties of Au NCs-$Ag@SiO_2$ Nanocomposites. To confirm the PEC enhancement capability of plasmonic Ag and the influence of distance, PEC tests were carried out first. As is presented in Figure 2A, compared with Au NCs/FTO

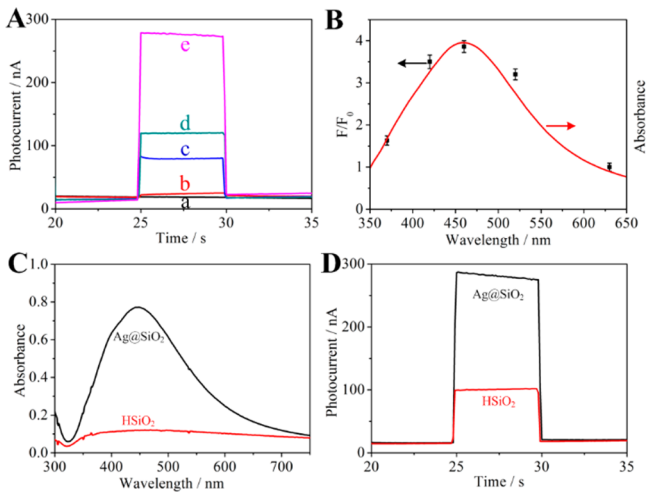

Figure 2. (A) Photocurrent responses of bare electrode (a), $Ag@SiO_2$/FTO (b), Au NCs/FTO (c), Au NCs-Ag NPs/FTO (d), and Au NCs-$Ag@SiO_2$ NPs/FTO (e). (B) Wavelength dependence of F/F_0 (solid squares), and the extinction spectrum of $Ag@SiO_2$ (solid line). (C) UV–vis spectra and (D) PEC properties of Au NCs-$Ag@SiO_2$ and Au NCs- $HSiO_2$ with a silica shell of 15 nm.

(curve c), the PEC responses of Au NCs-Ag/FTO (curve d) increased slightly, indicating that plasmon-mediated hot electron transfer between Ag NPs and adjacent Au NCs was helpful for efficient charge separation.[24] In this phenomenon, Ag NPs acts as a dye sensitizer, transferring SPR excited electrons to the nearby Au NCs for enhancing the photocurrent.[33] Detailly, the hot electrons of plasmonic Ag NPs were photoexcited to surface plasmon states, while the electrons

https://dx.doi.org/10.1021/acs.analchem.9b05432
Anal. Chem. 2020, 92, 6886–6892

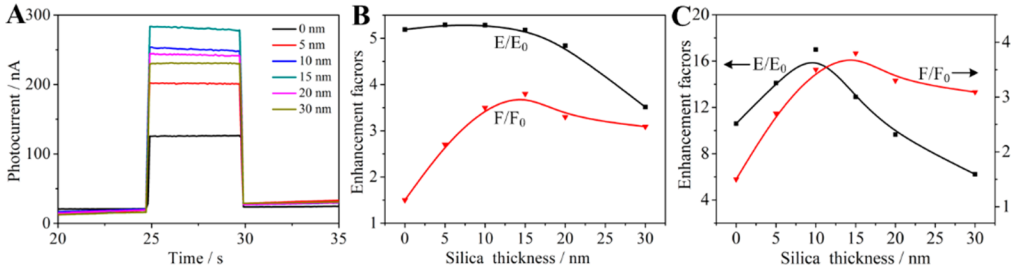

Figure 3. (A) Photocurrent responses of Au NCs-Ag@SiO_2/FTO. Comparison of the theoretical electric field of (B) Ag@SiO_2 monomers (C) Ag@SiO_2–Ag@SiO_2 dimers with the experimental photocurrent enhancement factors for Au NCs with different silica shell thicknesses.

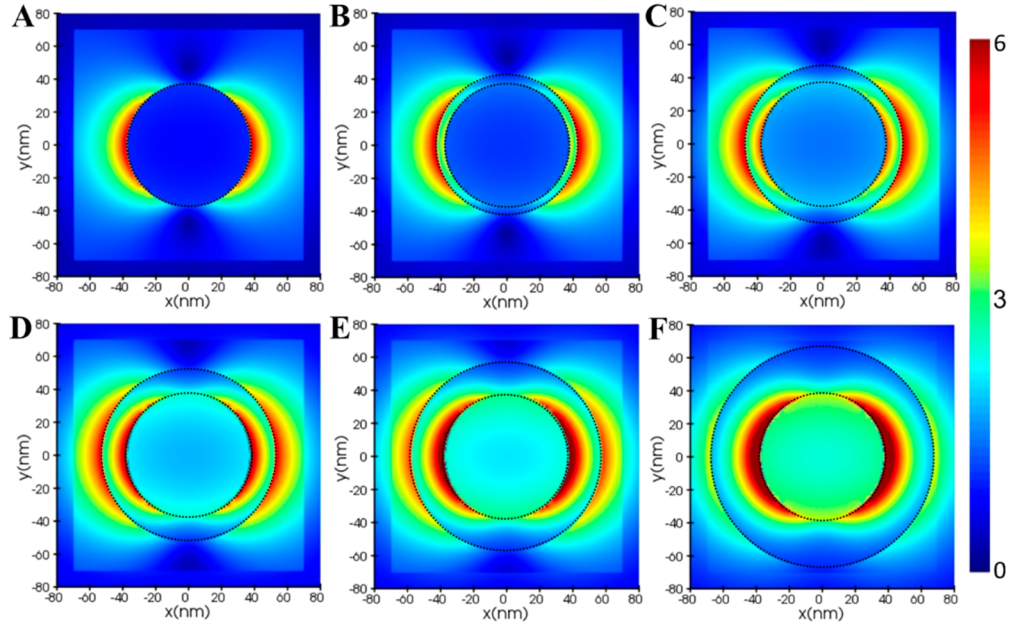

Figure 4. Electric field distribution around Ag@SiO_2 monomers (core, 75 nm in diameter) with (A) 0 nm, (B) 5 nm, (C) 10 nm, (D) 15 nm, (E) 20 nm, and (F) 30 nm silica shell thicknesses.

(e^-) of the Au NCs were transferred from the occupied highest occupied molecular orbital (HOMO) to the empty lowest unoccupied molecular orbital (LUMO).[34,35] Hereafter, the produced hot electrons would inject to the LUMO of Au NCs, and further transfer to the counter electrode (Pt) for hydrogen and photocurrent generation. The resulted photogenerated holes (h^+) and hot holes would be reduced by the electron donor (AA) in the solution. In this situation, Au NCs were attached on Ag NPs directly. While the transfer of hot electron would be suppressed when Au NCs were separated with Ag NPs by silica due to rapidly decaying energy of hot electron.[36] More significantly, the photocurrent intensity of Au NCs-Ag@SiO_2/FTO (curve e) enhanced obviously, illustrating SPR induced local electric field and light scattering may play an important role in the photocurrent enhancement.[37] Then, action spectra of photocurrent were discussed. As shown in Figure 2B, the spectral profile of the photocurrent enhancement factor (photocurrent ratio of Au NCs-Ag@SiO_2/FTO to Au NCs/FTO, F/F_0) was roughly in agreement with the shape of the LSPR peak of Ag@SiO_2, indicating that LSPR excitation of Ag core particles played an important role in the photoexcitation enhancement of Au NCs. Meanwhile, it was further certified by dissolving the Ag cores with sodium chloride to prepare the control samples (hollow silica nanoshells, $HSiO_2$).[38] After Ag cores were etched (Figure 2C), the photocurrent of Au NCs-$HSiO_2$/FTO significant decreased (Figure 2D), which illustrated that the increased PEC response toward AuNCs-Ag@SiO_2/FTO was ascribed to the SPR of Ag NPs.

To reveal the effect of AA and obtain a better photoelectric performance, influence of AA, Au NCs and Ag@SiO_2 NPs in Au NCs-Ag@SiO_2 nanocomposites were first performed (SI Figures S2 and S3). Based on these, all the following tests were carried out under the optimal conditions of fixed amounts of Au NCs (0.2 mg·mL^{-1}) and Ag@SiO_2 NPs (4.13×10^{-10} mol·L^{-1}) in composites. Noteworthy, the quantitative measurement was highly dependent on the coverage and aggregation status of Au NCs-Ag@SiO_2 on the electrode. It is reported that the photoelectric performance of semiconductors of nearby plasmonic-metal nanoparticles were distance-related.[31] Thus, the research on silica shell thickness was an important project for PEC enhancement. As shown in Figure 3A, the photocurrent responses of Au NCs-Ag@SiO_2/FTO with various thickness of silica shells were tested. It increased first and then decreased with the increasing silica shell thickness, and reached the maximum (3.8 times of Au NCs/FTO) at 15 nm (Figure 3B). The distance-dependent photoelectric performance was suspected due to changed contributions of hot electron transfer, local electric field, light scattering effects, and nonradiative energy transfer.

https://dx.doi.org/10.1021/acs.analchem.9b05432
Anal. Chem. 2020, 92, 6886−6892

Possible Enhancement Mechanism. The mechanisms of photoelectric enhancement were discussed, mainly due to reinforcing functions of hot electron transfer, local electric field, light scattering effects competed with the quenching functions of energy transfer in different distances. Especially, the intensity distributions of local electric field near Ag@SiO_2 monomers with different silica shell thicknesses in the $x-y$ plane under 460 nm light excitation were simulated. Moreover, the simulations for Ag@SiO_2−Ag@SiO_2 dimers were also carried out to consider the coupling effect. As shown in Figure 4 and SI Figure S4A−F, the black circles on each panel were signed to depict the distance between Ag core and silica shell, color scale bar represents relative enhancement of electric field intensity. The electric field intensities of silica surface decayed for monomeric particle increased within 10 nm and then decreased for dimeric particles with the increasing silica shell thickness. Noteworthy, the nonradiative energy transfer was also distance dependent and could be expressed within a Förster-like energy transfer mechanism by nonradiative dipole−dipole interaction. Correspondingly, the quenching effects of energy transfer would decline dramatically as the distances increased due to the transfer rate that was inversely proportional to the sixth power of the distance.[39,40] Differently, the hot electron transfer worked only when Ag NPs and Au NCs were connected directly, scattering effects took similar effects under different silica thicknesses, and the photoelectric enhancement of them mainly occurred in the far-field region.[41]

Based on this, the contribution of four effects were analyzed exhaustively through comparing F/F_0 obtained by experiment and electric field enhancement factor ($|E/E_0|$) of single side of silica surface for monomeric particle and gap for dimeric particles achieved by calculation. To better correlate the theoretical with experimental, the electric field enhancement at a fixed distance of 2 nm from the silica surface was taken as a function of calculation with the experiment. As shown in Figure 3B,C, when the silica thickness was 0 nm, the photocurrent enhancement factor was much lower, and slightly greater than 1. This was possible due to hot electron transfer and the local electromagnetic field competed with nonradiative energy transfer and dominated. Then, when the silica thicknesses were greater than 0 and less than 15 nm, the photocurrent enhancement factor increased more sharply. This might be because to the local electromagnetic field competed with nonradiative energy transfer and dominated. Finally, the photocurrent enhancement factors dropped more slowly when the silica thicknesses were over 15 nm. This was mainly due to the impact of far-field scattering effects taking place in the far-field region.

Characterizations of Biosensor. To prove the successful construction of the PEC biosensor, the EIS measurements were performed to characterize it step by step. In the EIS (Figure 5A), the values of semicircle diameters can directly reflect the electron-transfer resistance (R_{et}) levels of the modified electrodes. When the FTO electrode surface was modified with CS-Au NCs-Ag@SiO_2 nanomaterials (red line) and ALP in order, the R_{et} increased gradually, ascribed to poor conductivity of the nanomaterials and steric hindrance of protein molecules. PEC characterization was conducted to monitor the feasibility of sensor construction. As shown in Figure 5B, the photocurrent response of CS-Au NCs-Ag@SiO_2/FTO partly decreased after the modification of ALP, which was consistent with EIS characterization. In the presence of AAP, the photocurrent response showed a visible increase

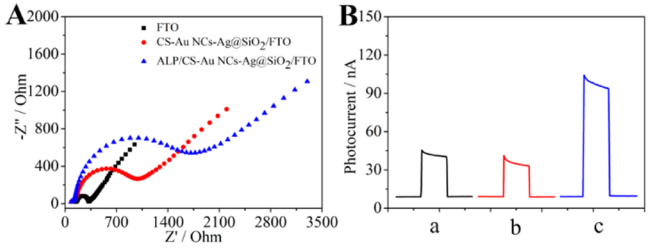

Figure 5. (A) EIS Nyquist plots of the stepwise fabrication for the PEC biosensors. (B) Photocurrent responses of (a) CS-Au NCs-Ag@SiO_2/FTO, (b) ALP/CS-Au NCs-Ag@SiO_2/FTO in buffer without AAP, and (c) ALP/CS-Au NCs-Ag@SiO_2/FTO in buffer with 40 mM AAP.

compared to that without AAP. This indicated that ALP can effectively hydrolyze AAP into AA, which act as an electron donor for scavenging photogenerated holes. The variation trend of the EIS and PEC output confirmed that the biosensor was successfully fabricated, and the values of enzymatic activity would be directly reflected by the levels of photocurrent increase.

Analytical Performance of the PEC Sensor. Under optimal conditions (SI Figure S5), the resulting PEC biosensor was used to investigate the ALP activity. As shown in Figure 6A, the photocurrent responses increased gradually with the

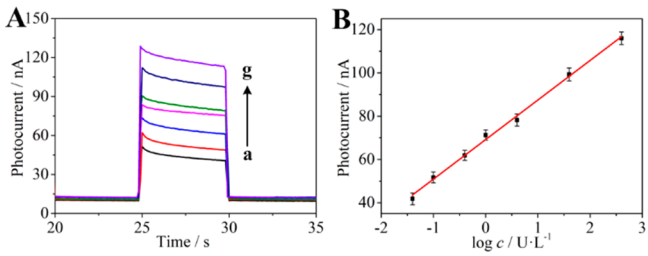

Figure 6. (A) Photocurrent response of the proposed PEC biosensor to ALP with different activities (a-g): 0.04, 0.1, 0.4, 1, 4, 40, 400 U·L^{-1}. (B) The as-derived calibration curve for ALP activity assay.

increasing ALP activity, due to stronger ALP activity that would catalyze hydrolysis AAP to generate more AA in situ. Moreover, the photocurrent responses showed a good linear proportional to the logarithm of the ALP activity (Figure 6B) with a regression equation of $i = 18.27 \log c_{ALP} + 69.20$ (R^2 = 0.9956). The corresponding linear range was from 0.04 to 400 U·L^{-1} with a detection limit of 0.022 U·L^{-1} (S/N = 3), which was comparable to that in previous references (SI Table S1).

To investigate selectivity of the proposed sensor, potential interferences including albumin from bovine serum (BSA), glucose oxidase (GOx), acetylcholinesterase (AChE), rabbit antihuman IgG (IgG), glucose (Glu), alanine (Ala), L-methionine (L-met), urea, Na^+, and K^+ were employed. As shown in SI Figure S6, only ALP could cause an obvious change toward photocurrent, and other potential disturbances showed negligible influences. The good specificity of the established detection platform was ascribed to the specific catalysis of ALP to AAP. Additionally, the reproducibility and stability were also investigated. For five independently fabricated biosensors, the relative standard deviation was calculated to be 5.2%, indicating good reproducibility of the biosensing platform. Noteworthy, the modified electrode still

https://dx.doi.org/10.1021/acs.analchem.9b05432
Anal. Chem. 2020, 92, 6886−6892

retained 91% of functions after storing in the dark at 4 °C for 7 days, implying excellent stored stability of the photoelectrode.

The practical applicability of the proposed PEC sensor was major theme of the research. Thus, we evaluated the ALP activity in 100-fold diluted human serum samples by the standard-addition method. As shown in SI Table S2, the recoveries for the serum samples ranged from 97.5% to 105.3%, with the RSDs ranging from 4.7% to 6.1%. These results implied that the designed PEC biosensor could be applied for quantitative assays in real biological samples.

CONCLUSION

In summary, the photoelectric properties of Au NCs was improved when they were integrated with Au@SiO_2 NPs. The photocurrent enhanced to its maximum at the optimum distance (ca. 15 nm) between Au NCs and Ag NPs in the presence of AA as an electron donor. The enhanced hot electron transfer, local electric field and light scattering effects are the sole mechanism responsible for the improvement of photoelectric performance. With the aid of ALP catalytic chemistry, the photoelectrodes were successfully applied to highly selective and sensitive ALP assay. The combination of experimental and theoretical aspects promotes insight into the mechanistic understanding of metal-enhanced photoelectric properties of semiconductors, which play a guiding role in designing and controlling of plasmonic nanostructures for advisible photoelectric signal enhancement. Simultaneously, the research is hoped to broaden application potential of nontoxic and biocompatible Au NCs in PEC bioanalysis.

ASSOCIATED CONTENT

Supporting Information

aThe Supporting Information is available free of charge at https://pubs.acs.org/doi/10.1021/acs.analchem.9b05432.

Reagents and materials, instruments, preparation procedures of Ag NPs, Ag@SiO_2 NPs, Au NCs, TEM image of Au NCs, UV−vis spectra of Ag NPs, Ag@SiO_2 NPs, Au NCs, and fluorescence spectrum of Au NCs, effect of AA, Au NCs and Ag@SiO_2 NPs on PEC response of Au NCs, Electric field distribution for Ag@SiO_2−Ag@SiO_2 dimers, optimization of experiment conditions for the PEC sensing, selectivity of the PEC biosensor, comparison the proposed PEC biosensor with previously reports, ALP activity assay in human blood serum samples (PDF)

AUTHOR INFORMATION

Corresponding Author

Shou-Nian Ding − *Jiangsu Province Hi-Tech Key Laboratory for Bio-medical Research, School of Chemistry and Chemical Engineering, Southeast University, Nanjing 211189, China;* orcid.org/0000-0003-3086-2333; Email: snding@seu.edu.cn; Fax: (+86) 25-52090621

Authors

Chun-Qin Zhao − *Jiangsu Province Hi-Tech Key Laboratory for Bio-medical Research, School of Chemistry and Chemical Engineering, Southeast University, Nanjing 211189, China*

Jing Zhou − *Jiangsu Province Hi-Tech Key Laboratory for Bio-medical Research, School of Chemistry and Chemical Engineering, Southeast University, Nanjing 211189, China*

Kai-Wen Wu − *Jiangsu Province Hi-Tech Key Laboratory for Bio-medical Research, School of Chemistry and Chemical Engineering, Southeast University, Nanjing 211189, China*

Jing-Juan Xu − *State Key Laboratory of Analytical Chemistry for Life Science and Collaborative Innovation Center of Chemistry for Life Sciences, School of Chemistry and Chemical Engineering, Nanjing University, Nanjing 210023, China;* orcid.org/0000-0001-9579-9318

Hong-Yuan Chen − *State Key Laboratory of Analytical Chemistry for Life Science and Collaborative Innovation Center of Chemistry for Life Sciences, School of Chemistry and Chemical Engineering, Nanjing University, Nanjing 210023, China*

Complete contact information is available at: https://pubs.acs.org/10.1021/acs.analchem.9b05432

Notes

The authors declare no competing financial interest.

ACKNOWLEDGMENTS

This work was supported by the National Key Research and Development Program of China (2017YFA0700404), the National Natural Science Foundation of China (21535003, 21575022), the Key Research & Development Plan of Jiangsu Province (BE2018617), the Fundamental Research Funds for the Central Universities (2242016K41055), and Key Laboratory of Optic-electric Sensing and Analytical Chemistry for Life Science, MOE, Qingdao University of Science and Technology (STAM201801), the Postgraduate Research & Practice Innovation Program of Jiangsu Province (KYCX19_0073).

REFERENCES

(1) Zhao, W.-W.; Xu, J.-J.; Chen, H.-Y. *Chem. Soc. Rev.* **2015**, *44*, 729−741.
(2) Zhang, N.; Ma, Z.-Y.; Ruan, Y.-F.; Zhao, W.-W.; Xu, J.-J.; Chen, H.-Y. *Anal. Chem.* **2016**, *88*, 1990−1994.
(3) Zhao, C.-Q.; Ding, S.-N. *Coord. Chem. Rev.* **2019**, *391*, 1−14.
(4) Zhao, W.-W.; Yu, X.-D.; Xu, J.-J.; Chen, H.-Y. *Nanoscale* **2016**, *8*, 17407−17414.
(5) Wang, G.-L.; Yuan, F.; Gu, T.; Dong, Y.; Wang, Q.; Zhao, W.-W. *Anal. Chem.* **2018**, *90*, 1492−1497.
(6) Liu, S.; Xu, Y. J. *Sci. Rep.* **2016**, *6*, 22742.
(7) Chen, Y. S.; Kamat, P. V. *J. Am. Chem. Soc.* **2014**, *136*, 6075−6082.
(8) Fan, G.-C.; Zhu, H.; Du, D.; Zhang, J.-R.; Zhu, J.-J.; Lin, Y. *Anal. Chem.* **2016**, *88*, 3392−3399.
(9) Zhang, J.; Tu, L.; Zhao, S.; Liu, G.; Wang, Y.; Wang, Y.; Yue, Z. *Biosens. Bioelectron.* **2015**, *67*, 296−302.
(10) Wang, S.-S.; Zhao, X.-P.; Liu, F.-F.; Younis, M. R.; Xia, X.-H.; Wang, C. *Anal. Chem.* **2019**, *91*, 4413−4420.
(11) Wang, C.; Nie, X.-G.; Shi, Y.; Zhou, Y.; Xu, J.-J.; Xia, X.-H.; Chen, H.-Y. *ACS Nano* **2017**, *11*, 5897−5905.
(12) Wang, C.; Zhao, X.-P.; Xu, Q.-Y.; Nie, X.-G.; Younis, M. R.; Liu, W.-Y.; Xia, X.-H. *ACS Appl. Nano Mater.* **2018**, *1*, 5805−5811.
(13) Li, R.; Tu, W.; Wang, H.; Dai, Z. *Anal. Chem.* **2018**, *90*, 9403−9409.
(14) Luo, Z. B.; Zhang, L. J.; Zeng, R. J.; Su, L. S.; Tang, D. P. *Anal. Chem.* **2018**, *90*, 9568−9575.
(15) Kim, J. K.; Jang, D.-J. *J. Mater. Chem. C* **2017**, *5*, 6037−6046.
(16) Wang, Z.; Liu, J.; Liu, X.; Shi, X.; Dai, Z. *Anal. Chem.* **2019**, *91*, 830−835.
(17) Cushing, S. K.; Li, J. T.; Meng, F. K.; Senty, T. R.; Suri, S.; Zhi, M. J.; Li, M.; Bristow, A. D.; Wu, N. Q. *J. Am. Chem. Soc.* **2012**, *134*, 15033−15041.

(18) Li, C. P.; Wang, P.; Li, H. J.; Wang, M. M.; Zhang, J.; Qi, G. H.; Jin, Y. D. *Nanoscale* **2018**, *10*, 14290−14297.
(19) Torimoto, T.; Horibe, H.; Kameyama, T.; Okazaki, K.-i.; Ikeda, S.; Matsumura, M.; Ishikawa, A.; Ishihara, H. *J. Phys. Chem. Lett.* **2011**, *2*, 2057−2062.
(20) Li, X.; Suzuki, K.; Toda, T.; Yasuda, S.; Murakoshi, K. *J. Phys. Chem. C* **2015**, *119*, 22092−22101.
(21) Liu, S. H.; Hou, Y. D.; Xie, W.; Schlucker, S.; Yan, F.; Lei, D. Y. *Small* **2018**, *14*, 12.
(22) Kumar, M. K.; Krishnamoorthy, S.; Tan, L. K.; Chiam, S. Y.; Tripathy, S.; Gao, H. *ACS Catal.* **2011**, *1*, 300−308.
(23) Yip, C. T.; Liu, X. L.; Hou, Y. D.; Xie, W.; He, J. J.; Schlucker, S.; Lei, D. Y.; Huang, H. T. *Nano Energy* **2016**, *26*, 297−304.
(24) Duchene, J. S.; Williams, B. P.; Johnston-Peck, A. C.; Qiu, J.; Gomes, M.; Amilhau, M.; Bejleri, D.; Weng, J.; Dong, S.; Huo, F. *Adv. Energy Mater.* **2016**, *6*, 1501250.
(25) Xiao, F. X.; Zeng, Z.; Liu, B. *J. Am. Chem. Soc.* **2015**, *137*, 10735−10744.
(26) Kogo, A.; Takahashi, Y.; Sakai, N.; Tatsuma, T. *Nanoscale* **2013**, *5*, 7855−7860.
(27) Wang, X.; Liu, Z.; Zhao, W.; Sun, J.; Qian, B.; Wang, X.; Zeng, H.; Du, D.; Duan, J. *Anal. Bioanal. Chem.* **2019**, *411*, 1009−1017.
(28) Wang, S.; Zhao, J.; Zhang, Y.; Yan, M.; Zhang, L.; Ge, S.; Yu, J. Photoelectrochemical Biosensor of HIV-1 Based on Cascaded Photoactive Materials and Triple-Helix Molecular Switch. *Biosens. Bioelectron.* **2019**, *139*.111325
(29) Lee, P. C.; Meisel, D. *J. Phys. Chem.* **1982**, *86*, 3391−3395.
(30) Yang, J.; Zhang, F.; Chen, Y.; Qian, S.; Hu, P.; Li, W.; Deng, Y.; Fang, Y.; Han, L.; Luqman, M.; Zhao, D. *Chem. Commun.* **2011**, *47*, 11618−11620.
(31) Luo, Z. T.; Yuan, X.; Yu, Y.; Zhang, Q. B.; Leong, D. T.; Lee, J. Y.; Xie, J. P. *J. Am. Chem. Soc.* **2012**, *134*, 16662−16670.
(32) Zhang, X.; Du, X. *ACS Appl. Mater. Interfaces* **2016**, *8*, 1033−1040.
(33) Warren, S. C.; Thimsen, E. *Energy Environ. Sci.* **2012**, *5*, 5133−5146.
(34) Ruan, Y.-F.; Zhang, N.; Zhu, Y.-C.; Zhao, W.-W.; Xu, J.-J.; Chen, H.-Y. *Anal. Chem.* **2017**, *89*, 7869−7875.
(35) Shi, Y.; Wang, J.; Wang, C.; Zhai, T.-T.; Bao, W.-J.; Xu, J.-J.; Xia, X.-H.; Chen, H.-Y. *J. Am. Chem. Soc.* **2015**, *137*, 7365−70.
(36) Linic, S.; Christopher, P.; Ingram, D. B. *Nat. Mater.* **2011**, *10*, 911−921.
(37) Standridge, S. D.; Schatz, G. C.; Hupp, J. T. *J. Am. Chem. Soc.* **2009**, *131*, 8407−8409.
(38) Lessard-Viger, M.; Rioux, M.; Rainville, L.; Boudreau, D. *Nano Lett.* **2009**, *9*, 3066−3071.
(39) Zhang, X.; Marocico, C. A.; Lunz, M.; Gerard, V. A.; Gun'ko, Y. K.; Lesnyak, V.; Gaponik, N.; Susha, A. S.; Rogach, A. L.; Bradley, A. L. *ACS Nano* **2012**, *6*, 9283−9290.
(40) Clapp, A. R.; Medintz, I. L.; Mauro, J. M.; Fisher, B. R.; Bawendi, M. G.; Mattoussi, H. *J. Am. Chem. Soc.* **2004**, *126*, 301−310.
(41) Liu, S.; Yidong, H.; Wei, X.; Sebastian, S.; Feng, Y.; Yuan, L. D. *Small* **2018**, *14*, 1800870.

https://dx.doi.org/10.1021/acs.analchem.9b05432
Anal. Chem. 2020, 92, 6886−6892